CHAPTER 6
THERMODYNAMIC MODELLING AND ANALYSIS OF COMBINED RRVPC AND BOILER FLUE GAS DRIVEN DOUBLE EFFECT H_2O–LiBr VARS

6.1 Introduction

Towards the end of the previous chapter, it was mentioned that the boiler leaving flue gas exhaust heat could be a source of heat for vapor generation in a VARS. In thermal power plants, to recover waste heat and improve plant efficiency further, hot flue gas are often used for preheating of boiler feed water and combustion air separately in an economizer and air–preheater respectively. Similarly, the hot flue gas can also be used for driving the generator of the VARS. Certainly a question arises at this stage as to which VARS configuration would be appropriate for heat integration with the flue gas exhaust as there are several VARS configurations available, starting from half effect to triple effect. Some of these VARS configurations were discussed with their schematic in Chapter 1. Amongst all these configurations, the single effect VARS is the most commonly used refrigeration system. Multi effect (double and triple effect) VARS are also receiving significant attention as they offer higher COP and are efficient in utilizing heat source of relatively high temperature.

The double effect absorption refrigeration cycle was conceptualized during 1956–1958 [1]. It has more commercial use in the refrigeration industry than the triple effect systems [2, 3] due to increased cost and system complexity associated with the later. Over the years, many studies have been performed on double effect H_2O–LiBr refrigeration systems, while some of them deal with the energetic performance analysis [4–11] and some other articles [12–18] are specific to exergy analysis. Most of these studies related to double effect H_2O–LiBr VARS [2, 3, 10, 11, 13–16, 19–26] performance analysis were reviewed and discussed in Chapter 2.

Often ARSs are coupled with other systems that provide the driving heat source, e.g. the articles [27–30] discussed in Chapter 2, deal with solar powered single effect H_2O–LiBr VARS. Similarly, the articles [7, 31] reviewed in Chapter 2 were based on solar energy driven double effect H_2O–LiBr absorption system. The work of Havelsky [32] and some other works [33–38] which were categorically mentioned in Section 2.4.2.1 of Chapter 2 provided energetic performance analysis of single effect NH_3–H_2O

and H_2O–LiBr based VARS driven by ICE exhaust gas heat except the article [33] where the system analysis was done also from exergetic and economic point of view. Thermodynamic analyses done on GT/MGT exhaust driven VARS [39–47] were also discussed in Chapter 2 in section 2.4.2.2. Some of the studies discussed in Chapter 2 were specific to analysis of CPC systems involving double effect H_2O–LiBr VARS [7, 31, 39–41, 43]. There is no article in the literature that combines a steam based VPC and boiler flue gas energized double effect H_2O–LiBr VARS.

Therefore, a combined VPC and boiler flue gas driven double effect H_2O–LiBr absorption refrigeration system (ARS) is proposed in this chapter. Energy and exergy analyses of the proposed system are performed to evaluate its thermodynamic performance. A parametric analysis is carried out to show energetic and exergetic performance variation with flue gas temperature (hence also HPG temperature of the double effect ARS). Further a performance comparison is provided between two combined power and absorption cooling systems, one with the double effect H_2O–LiBr VARS as a bottoming cycle and the other with a single effect VARS. Double effect ARS has the advantage of higher COP over single effect systems, but the number of components are more. Therefore, the comparative study is done to determine exactly the difference in performance of the two combined systems also from exergy point of view under the condition of same flue gas temperature. It is apparently obvious that when the flue gas is used for operating single effect VARS, it would cause large irreversible losses due to larger temperature difference between flue gas and generator temperature of VARS. But in double effect system, the loss would be somewhat less due to lesser temperature difference between flue gas and generator (HPG) temperature.

6.2 Model description of the combined VPC and double effect H_2O–LiBr VARS

Fig.6.1 shows the schematic of the combined VPC and the double effect H_2O–LiBr VARS. The reheat regenerative type coal fired VPC with one open water heater (OWH), one closed water heater (CWH) and the reheater is the topping cycle and the double effect H_2O–LiBr VARS is the bottoming cycle of the combined system (CS). The topping VPC is similar to the one described in chapter 3, however in this schematic the exhaust heat of the boiler leaving flue gas is utilized for driving the double effect H_2O–LiBr VARS.

Fig.6.2 shows the schematic of the combined VPC and the single effect H_2O–LiBr VARS. It is seen that Fig.6.2 is more or less similar to Fig. 3.1 (in Chapter 3); the only difference is that now here in this schematic, heat is supplied by boiler flue gas exhaust and since it is a double effect system, therefore the number of components are more.

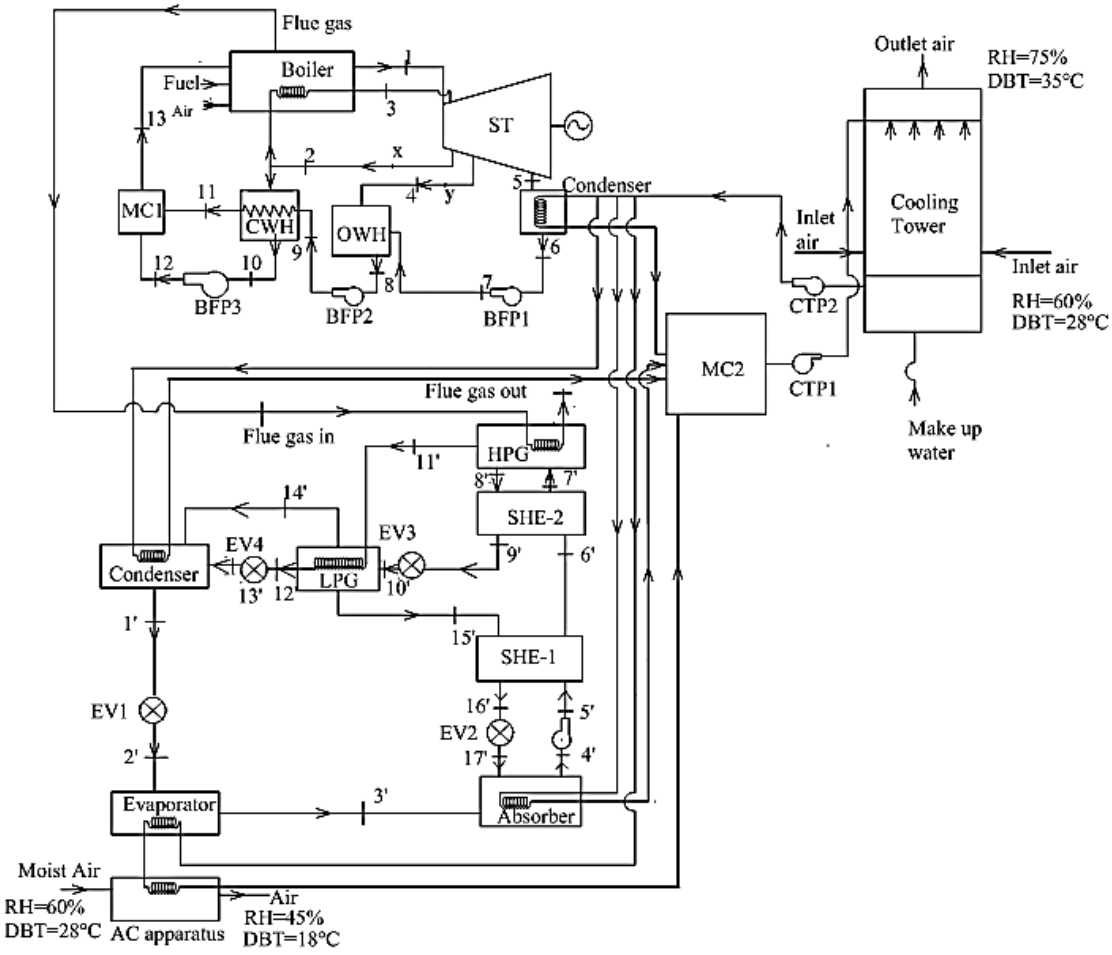

Fig.6.1: Layout of combined vapor power cycle and double effect H_2O–LiBr VARS.

The double effect H_2O–LiBr VARS is of series flow configuration with two generators (HPG and LPG), condenser, evaporator, absorber, solution pump, two solution heat exchangers (SHEs), two solution reducing valves and two refrigerant expansion valves. The source of heat for the HPG of the double effect H_2O–LiBr VARS is the boiler leaving hot flue gas. No external source of heat is utilized for vapour generation in the LPG. The HPG off primary vapour provides the latent heat of condensation required for generation of secondary vapour in the LPG from HPG off medium concentration solution.

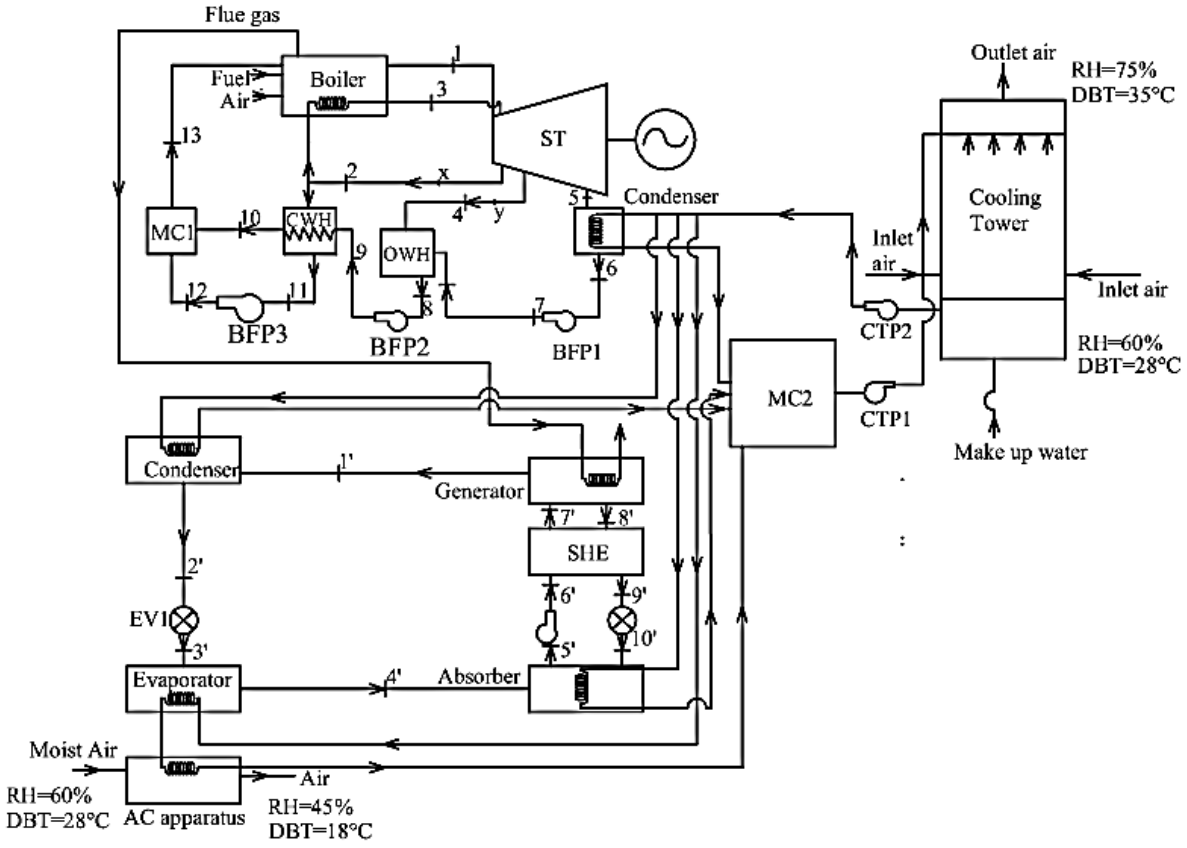

Fig.6.2: Layout of combined vapor power cycle and single effect H_2O–LiBr VARS.

The various parameters assumed for simulation of the combined power and double effect H_2O–LiBr VARS are shown in Table 6.1 (topping PC) and Table 6.2 (double effect H_2O−LiBr VARS).

Table 6.1: Operating parameters of the ST based power cycle

Parameter	Value
Fuel (Coal) flow rate	20 kg/s
Boiler pressure	150 bar
STIT	500°C
ST isentropic efficiency	85%
Reheat pressure	30 bar
CWH pressure	30 bar
OWH pressure	3.106 bar
Pump isentropic efficiency	85%
Condenser pressure	0.1 bar
CWH terminal temperature	3°C
CT exit water temperature	25°C
CT inlet air temperature	28°C
CT inlet air relative humidity	60%
CT exit air temperature	35°C
CT exit air relative humidity	75%
Flue gas temperature at boiler exit	130°C−160°C

Table 6.2: Operating parameters of the double effect $H_2O-LiBr$ ARS

Parameter	Value
Evaporator cooling capacity	500 ton
HPG temperature	120°C −150°C
LPG temperature	80°C
ARS condenser temperature	35°C
Evaporator temperature	10°C
Absorber temperature	35°C
SHEs' effectiveness	70%
Condenser, evaporator, absorber inlet water temperature	25°C
Condenser exit water temperature	30°C
Evaporator exit water temperature	10°C
Absorber exit water temperature	30°C
Chilled water temperature at AC apparatus inlet	10°C
Air mass flow rate through AC apparatus	4 kg/s
AC apparatus inlet air temperature	28°C
AC apparatus exit air temperature	18°C
AC apparatus inlet air relative humidity	60%
AC apparatus exit air relative humidity	45%

6.3 Governing equations for thermodynamic modelling of RRVPC

Same coal composition as mentioned in Chapter 3 is used and complete fuel combustion is assumed. The combustion gases comprise of CO_2, H_2O, SO_2, and N_2 in the product and they are treated as ideal gas mixture. For the molar specific heat of the combustion gases, the following temperature dependent model is adopted.

$$\frac{C_p}{R} = a_1 + a_2 T + a_3 T^2 + a_4 T^3 + a_5 T^4 \tag{6.1}$$

The values of the coefficients a_1, a_2, a_3, a_4 and a_5 for the combustion gases are known [48]. Mass flow rate and mass based specific heat of the combustion flue gases are determined as follows.

$$\dot{m}_{fg} = \sum_i \dot{n}_i M_i \tag{6.2}$$

$$C_{p,fg} = \sum_i Y_i \frac{C_{p,i}}{M_i} \tag{6.3}$$

In the above equations, $\dot{n}_i$, Y_i and M_i are the rate of molar composition, mass fraction and molecular weight of different gaseous components respectively.

Chemical and thermo–mechanical exergy of air are calculated following the same procedure as outlined in chapter 4. Similarly, the same methodology as mentioned in chapter 5 was adopted for calculation of other parameters and the VPC component's irreversibility.

6.4 Governing equations for thermodynamic modelling of the double effect H_2O−LiBr VARS

The series flow type double effect water−LiBr VARS is modeled using the procedure and assumptions of Gomri and Hakimi [13]. The unknown temperatures of two fluid steams at the outlet of the two solution heat exchangers (SHEs) are calculated using effectiveness method. The effectiveness of both SHE1 and SHE2 are taken as 70%. The thermodynamic properties of water−LiBr solutions at various temperatures and concentrations are calculated using the correlations proposed by Patek and Klomfar [49].

The evaporator cooling load (CL) ($\dot{Q}_E$)is specified (500 ton) and refrigerant mass flow rate is calculated as follows.

$$\dot{m}_{H_2O} = \frac{\dot{Q}_E}{h_3' - h_2'} \tag{6.4}$$

Concentrations of the weak (as function of VARS condenser and LPG temperature) and strong solution (as function of the absorber and evaporator temperatures) are calculated using equations taken from the Ref. [50].

$$X_{ws} = \frac{49.04 + 1.125T_{LPG} - T_C}{134.65 + 0.47T_{LPG}} \tag{6.5}$$

$$X_{ss} = \frac{49.04 + 1.125T_A - T_E}{134.65 + 0.47T_A} \tag{6.6}$$

Concentration of the medium solution is calculated in an iterative manner until the energy balance in the LPG is satisfied [13]. Mass flow rates of the weak, medium and strong solutions can be calculated from known values of refrigerant mass flow rate and their respective concentrations. The AC apparatus is analyzed and the temperature of the mixed water stream at MC2 exit is calculated in the same way as described in chapter 4.

The following is the energy balance equation in the LPG.

$$\dot{Q}_{LPG} = \dot{m}_{10}h'_{10} + \dot{m}_{11}h'_{11} = \dot{m}_{12}h'_{12} + \dot{m}_{14}h'_{14} + \dot{m}_{15}h'_{15} \quad (6.7)$$

The heat load in the HPG can be expressed as:

$$\dot{Q}_{HPG} = \dot{m}_8 h'_8 + \dot{m}_{11}h'_{11} - \dot{m}_7 h'_7 \quad (6.8)$$

The heat load in the condenser can be expressed as:

$$\dot{Q}_C = \dot{m}_{13}h'_{13} + \dot{m}_{14}h'_{14} - \dot{m}_{H_2O}h'_1 \quad (6.9)$$

The heat load in the absorber can be expressed as:

$$\dot{Q}_A = \dot{m}_{H_2O}h'_3 + \dot{m}_{17}h'_{17} - \dot{m}_{ss}h'_4 \quad (6.10)$$

In the VARS modeling, the flue gas temperature at HPG inlet ($T_{fg,HPGi}$) is specified which is actually the temperature of flue gas at boiler exit. This is varied in the range from 130°C to 160°C. However, the flue gas temperature at HPG outlet ($T_{fg,HPGo}$) is not known before calculation of $\dot{Q}_{HPG}$, therefore first it is assumed and then specific heat values of flue gas at $T_{fg,HPGi}$ and $T_{fg,HPGo}$ are calculated using Equation (5.1) to find the average specific heat. HPG heat since it is supplied by the flue gas, can also be expressed as follows.

$$\dot{Q}_{HPG} = \dot{m}_{fg} C_{p,fg} \left(T_{fg,HPGi} - T_{fg,HPGo} \right) \quad (6.11)$$

From equation (6.11), it follows that the new value of flue gas temperature at HPG exit is:

$$T_{fg,HPGo,new} = T_{fg,HPGi} - \frac{\dot{Q}_{HPG}}{\dot{m}_{fg} C_{p,fg}} \tag{6.12}$$

This new value of $T_{fg,HPGo,new}$ is updated and calculation is repeated until the difference between two successive $T_{fg,HPGo,new}$ values becomes negligibly small. Once $T_{fg,HPGo}$ is determined, the exergy of the flue gas at the HPG exit can be determined.

Cooling water flow rate through the evaporator/AC apparatus, absorber and the VARS condenser are determined from heat balance applied to these devices. The COP and exergy efficiency of the VARS are defined as follows:

$$COP = \frac{\dot{Q}_E}{\dot{Q}_{HPG} + \dot{W}_{SP}} \text{ , } \dot{W}_{SP} \text{ be the solution pump work as defined below.} \tag{6.13}$$

$$\dot{W}_{SP} = \dot{m}_4 \frac{\left(p_{HPG} - p_C\right)}{\eta_{SP} \rho_4} \tag{6.14}$$

$$\text{VARS exergy efficiency} = \frac{\left(\dot{E}x_{w,Eo} - \dot{E}x_{w,Ei}\right)}{\left(\dot{E}x_{fg,HPGi} - \dot{E}x_{fg,HPGo}\right) + \dot{W}_{SP}} \tag{6.15}$$

Effective utilization factor (EUF) of the CS is defined as:

$$EUF = \frac{\dot{W}_{net} + \dot{Q}_E}{\dot{m}_f LHV_f} \tag{6.16}$$

Exergetic efficiency of the combined power and double effect water−LiBr ARS is defined by the following equation.

$$\eta_{II,CS} = \frac{\dot{W}_{net} + \dot{E}x_{w,Eo} - \dot{E}x_{w,Ei}}{\dot{E}x_{ch,f} + \dot{E}x_{tm,a} + \dot{E}x_{fg,HPGi} - \dot{E}x_{fg,HPGo}} \tag{6.17}$$

Irreversibility in the HPG and LPG:

$$\dot{I}_{HPG} = \dot{m}_7 ex'_7 - \dot{m}_8 ex'_8 - \dot{m}_{11} ex'_{11} + \dot{E}x_{fg,HPGi} - \dot{E}x_{fg,HPGo} \tag{6.18}$$

$$\dot{I}_{LPG} = \dot{m}_{11} ex'_{11} + \dot{m}_{10} ex'_{10} - \dot{m}_{12} ex'_{12} - \dot{m}_{14} ex'_{14} - \dot{m}_{15} ex'_{15} \tag{6.19}$$

where $ex' = \left(h' - h^0\right) - T_o\left(s' - s^0\right)$ is the specific exergy of the flow stream.

Same methods as specified in Chapter 4 are applied to calculate exergy destruction in the ARS condenser, expansion valves, evaporator, AC apparatus, absorber, solution reducing valves, SHEs etc.

6.5 Validation of double effect H_2O−LiBr VARS model

For validation of the model, the results obtained from simulation of double effect water–LiBr series configuration are compared with the previously published results of Gomri and Hakimi [13] and Farshi et al. [3]. The comparison is shown in Table 6.3 and Table 6.4. A good agreement between the present and the previously published results was observed except with little deviations in the enthalpy values at various state points and more particularly at state point 7. Due to this little change in the enthalpy value at state point 7, the HPG heat load also changed slightly in Table 6.4 and consequently, COP value was found slightly higher in this study than those of Gomri and Hakimi [13] and Farshi et al. [3] at same operating conditions. Since the strong and weak solution concentrations were calculated from Ref. [50], therefore, these were not exactly same with those of Ref. [3] and Ref. [13] and accordingly, the values of mass flow rate of the weak and strong solutions were also slightly different from Refs. [3,13].

The validation of model equations used for modeling topping VPC was provided in Chapter 3. Now, here in this chapter, it is seen that the results obtained from simulation of double effect VARS configuration don't deviate much from those of Ref. [3] and Ref. [13]; therefore, the developed models were used to simulate the proposed combined RRVPC and double effect VARS configuration. The results obtained from simulation of the proposed CPC system are presented in the following subsections.

Table 6.3: Comparison of present results with those of Gomri and Hakimi [13] and Farshi et al. [3] for the double effect series configuration

State Point	T (K)			$\dot{m}$ (kg/s)			X (%)			h (kJ/kg)	
	Gomri	Farshi	Present study	Gomri	Farshi	Present study	Gomri	Farshi	Present study	Farshi	Present study
1	308	308	308	0.127	0.127	0.127	-	-	-	146.59	146.018
2	277	277	277	0.127	0.127	0.127	-	-	-	146.59	146.018
3	277	277	277	0.127	0.127	0.127	-	-	-	2507.87	2507.96
4	308	308	308	1.737	1.735	1.693	55.869	55.88	55.88	87.67	87.41
5	308	308	308	1.737	1.735	1.693	55.869	55.88	55.88	87.67	87.45
6	335.49	335.4	336.36	1.737	1.735	1.693	55.869	55.88	55.88	143.14	144.66
7	379.81	379.8	381.31	1.737	1.735	1.693	55.869	55.88	55.88	235.43	238.32
8	403	403	403	1.671	1.67	1.627	58.056	58.07	58.12	288.40	288.23
9	349.09	356.0	356.35	1.671	1.67	1.627	58.056	58.07	58.12	192.49	192.96
10	349.09	356.0	356.35	1.671	1.67	1.627	58.056	58.07	58.12	192.49	192.96
11	403	403	403	0.065	0.065	0.065	-	-	-	2740.53	2740.76
12	355.46	355.4	355.34	0.065	0.065	0.065	-	-	-	345.21	344.15
13	308	308	308	0.065	0.065	0.065	-	-	-	345.21	344.15
14	353	353	353	0.062	0.062	0.062	-	-	-	2649.57	2649.76
15	353	353	353	1.61	1.608	1.566	60.278	60.29	60.41	195.84	196.19
16	321.67	321.6	321.5	1.61	1.608	1.566	60.278	60.29	60.41	135.98	136.15
17	321.67	321.6	321.5	1.61	1.608	1.566	60.278	60.29	60.41	135.98	136.15

Table 6.4: Comparison of component heat loads, SP power and COP of present study with those of Gomri and Hakimi [13] and Farshi et al. [3] at $T_C = T_A = 35\,°\text{C}$, $T_E = 4\,°\text{C}$, $T_{HPG} = 130\,°\text{C}$, $T_{LPG} = 80\,°\text{C}$, 70% SHE-I and SHE-II efficiencies and 95 % SP efficiency for the double effect series configuration

Parameter	Ref. [13]	Farshi [3]	Present study
HPG, ($\dot{Q}_{HPG}$ kW)	252.407	252.394	244.700
Condenser, $\dot{Q}_C$ kW	167.205	167.190	167.37
Evaporator, ($\dot{Q}_E$ kW)	300.000	300.000	300.000
Absorber, ($\dot{Q}_A$ kW)	385.236	385.203	383.74
SP, ($\dot{W}_{SP}$ kW)	$\approx$0.000	0.033	0.053
COP	1.189	1.188	1.226

6.6 Thermodynamic analysis of combined VPC and double effect water−LiBr VARS operated by boiler flue gas exhaust

The performance based results of the combined ST based power cycle and boiler flue gas driven double effect water−LiBr ARS are presented in this section. The various parameters assumed for simulation of the combined power and double effect H_2O–LiBr ARS are shown in Table 6.1 (topping PC) and Table 6.2 (double effect water−LiBr ARS). The HPG temperature was varied from 120°C to 150°C in a step of 10°C and simultaneously the flue gas temperature was also varied from 130°C to 160°C to maintain a minimum 10°C temperature difference between the flue gas and the HPG temperature. Table 6.5 shows the performance of the topping PC, bottoming double effect water−LiBr ARS and the CS at various HPG temperatures. Since the CL was fixed (500 ton), therefore the flue gas temperature at HPG exit changed accordingly i.e. when the flue gas enters the HPG at higher temperature, the HPG outlet flue gas temperature also becomes high. It was seen that the net power output from the topping PC decreases with increase in HPG temperature due to reduction in steam generation rate in the boiler. With a coal burning rate of 20 kg/s, the amount of steam generated in the boiler decreases from 183.056 kg/s at T_{HPG} =120°C to 180.785 kg/s at T_{HPG} =150°C. This was the main reason behind low net power output from the topping PC at higher HPG temperature. Actually with reduction in steam flow rate, not only the work developed by the ST $\left(\dot{W}_{ST}\right)$, but simultaneously the BFP and CT side pumping power also reduces, but overall the net power output decreases. Due to reduction in steam flow rate, energy loss in the PCC decreases and therefore less amount of cooling water is required to be circulated through the PCC which finally reduces the CT side pumping power. Energy and exergy efficiency of the topping PC also reduce with increase in HPG temperature due to reduction in the net power output.

Table 6.5: Performance of the combined power and double effect H_2O−LiBr ARS at various HPG temperatures

Performance parameters	HP Generator temperature (°C)			
	120	130	140	150
Flue Gas temperature at boiler exit/HPG inlet (°C)	130	140	150	160
Flue Gas temperature at HPG exit (°C)	123.61	133.52	143.43	153.35
Topping PC				
Net power (MW)	185.435	184.702	183.969	183.235
Steam generation rate (kg/s)	183.056	182.299	181.542	180.785
BFP pumping power (kW)	4233.471	4215.957	4198.444	4180.931
CT side pumping power (kW)	5589.673	5532.428	5475.570	5419.102
PC condenser loss (MW)	273.867	272.734	271.601	270.468
Energy efficiency of PC (%)	37.375	37.227	37.079	36.931
Exergy efficiency of PC (%)	35.241	35.102	34.963	34.823
Bottoming ARS				
COP	1.411	1.386	1.364	1.343
$\dot{Q}_{HPG}$ (kW)	1240.2	1262.0	1283.0	1302.7
$\dot{W}_p$ (W)	0.1405	0.2016	0.2829	0.3894
$\dot{Q}_C$ (kW)	931.0	955.9	980.6	1005.1
$\dot{Q}_A$ (kW)	2076.1	2076.1	2076.1	2076.1
$\dot{m}_{H_2O}$ (kg/s)	0.7376	0.7376	0.7376	0.7376
$\dot{m}_{LiBr}$ (kg/s)	2.7186	2.7186	2.7186	2.7186
$\dot{m}_{ws}$ (kg/s)	4.5009	4.5009	4.5009	4.5009
$\dot{m}_{ms}$ (kg/s)	4.8448	4.8493	4.8538	4.8584
$\dot{m}_{ss}$ (kg/s)	5.2385	5.2385	5.2385	5.2385
Exergy efficiency (%)	14.426	13.233	12.240	11.405
CS				
EUF of the CS (%)	37.727	37.580	37.432	37.284
Exergetic efficiency of CS (%)	35.229	35.088	34.947	34.805

It was also observed that COP of the double effect water−LiBr ARS reduces with increasing HPG temperature from 1.411 at T_{HPG} =120°C to 1.343 at T_{HPG} =150°C. That the COP of double effect water−LiBr ARS decreases with increasing HPG temperature was also reported by Gomri and Hakimi [13]. When the HPG temperature is increased, both the heat load in the HPG $\left(\dot{Q}_{HPG}\right)$ and the SP power increases, although the increase in SP power has little influence on COP compared to that of $\dot{Q}_{HPG}$. With increase in T_{HPG}, mass flow rates of the refrigerant, weak and strong solutions remain the same, only medium solution mass flow rate($\dot{m}_8'$)shows a slight increase. On the other hand, mass

flow rate of the primary vapor generated in the HPG ($\dot{m}'_{11}$) reduces slightly while $\dot{m}'_7$ remains unchanged. Specific enthalpies at state points $7'$, $8'$ and $11'$ increase with increase in T_{HPG}. All these variations finally cause an increase in $\dot{Q}_{HPG}$. SP pumping power increases mainly due to increase in HPG pressure which increases from 43.062 kPa at T_{HPG} =120°C to 117.176 kPa at T_{HPG} =150°C. Therefore, the COP of the double effect ARS reduces at higher HPG temperature. Of course this trend was mainly caused by the fixed LPG temperature which in the present analysis is 80°C, but otherwise the COP of the double effect system improves at higher LPG temperature [13]. Condenser heat load $(\dot{Q}_C)$also increases with T_{HPG} mainly due to increase in specific enthalpy value at state point $13'$ (h'_{13}) which increases from 325.047 kJ/kg at T_{HPG} =120°C to 436.402 kJ/kg at T_{HPG} =150°C (See Equation 6.9). Mass flow rate at state point $13'$ ($\dot{m}'_{13}$) slightly reduces while the mass flow rate at state point $14'$ $(\dot{m}'_{14})$shows a marginal increase and $\dot{m}'_1$ remains unchanged with T_{HPG}. As such, variation in $\dot{m}'_{13}$ and $\dot{m}'_{14}$ was not responsible for increase in $\dot{Q}_C$. Increase in $\dot{Q}_C$ demands more cooling water circulation through the ARS condenser. The main reason behind lower CT side pumping power at higher T_{HPG} was the reduction in water flow rate through the PCC because the PCC heat loss was more compared to $\dot{Q}_C$ of the ARS. Heat load in the absorber $(\dot{Q}_A)$is not affected by T_{HPG} variation. The exergy efficiency of the double effect ARS also decreases with increase in HPG temperature. The EUF and exergetic efficiency of the combined power and cooling system also shows a declining trend at higher T_{HPG}. This mainly happens due to reduction in the net power output of the topping PC.

Table 6.6: Components' irreversibility of the combined power and double effect water−LiBr ARS at various HPG temperatures.

Irreversibility(kW)	Notation	HP Generator temperature (°C) 120	130	140	150
Topping PC components					
Boiler	$\dot{I}_{boiler}$	222595.693	221009.457	219423.222	217836.987
Steam Turbine	$\dot{I}_{ST}$	20947.736	20861.078	20774.419	20687.760
PC condenser	$\dot{I}_{PCC}$	11242.480	11195.971	11149.462	11102.953
BFPs	$\dot{I}_{BFP}$	268.149	267.039	265.930	264.821
Open water heater	$\dot{I}_{OWH}$	4409.198	4390.958	4372.717	4354.477
Closed water heater	$\dot{I}_{CWH}$	3888.286	3872.201	3856.115	3840.029
Mixing chamber 1	$\dot{I}_{MC1}$	0	0	0	0
Mixing chamber 2	$\dot{I}_{MC2}$	244.712	245.384	246.048	246.706
Cooling tower	$\dot{I}_{CT}$	17726.555	17652.546	17578.540	17504.540
Cooling tower pumps	$\dot{I}_{CTP}$	21577.971	21278.585	20984.500	20695.417
Bottoming ARS components					
HP Generator	$\dot{I}_{HPG}$	30.152	30.608	31.203	31.878
LP Generator	$\dot{I}_{LPG}$	4.861	24.556	42.838	59.805
ARS condenser	$\dot{I}_{C}$	24.392	25.019	25.640	26.257
Expansion valve 1	$\dot{I}_{ExV1}$	3.390	3.390	3.390	3.390
Expansion valve 2	$\dot{I}_{ExV2}$	0	0	0	0
Expansion valve 3	$\dot{I}_{ExV3}$	4.325	6.128	8.184	10.471
Expansion valve 4	$\dot{I}_{ExV4}$	0	0	0	0
Evaporator	$\dot{I}_{E}$	47.125	47.125	47.125	47.125
Absorber	$\dot{I}_{A}$	101.992	101.992	101.992	101.992
Solution pump	$\dot{I}_{SP}$	0.1305	0.187	0.263	0.362
Solution heat exchanger 1	$\dot{I}_{SHE1}$	11.354	11.359	11.365	11.373
Solution heat exchanger 2	$\dot{I}_{SHE2}$	17.594	23.218	29.288	35.685
AC apparatus	$\dot{I}_{AC}$	1.724	1.724	1.724	1.724
Exhaust gas	$\dot{I}_{fg}$	52173.419	55071.036	57666.310	60263.370

The irreversible losses occurring in various system components of the topping PC and bottoming double effect water−LiBr ARS were determined applying exergy balance to each individual component of the CS. These are shown in Table 6.6 at various HPG temperatures. The irreversibility in the PC components decreases with increase in T_{HPG} due to reduction in steam generation rate at higher T_{HPG}. Irreversibility distribution

among various PC components showed that that the boiler contributes the maximum irreversibility followed by the CTPs, ST, CT, PC condenser, OWH, CWH, BFPs and the MC2 at all HPG temperatures.

The effect of variation of T_{HPG} on irreversibility of the ARS components was however just the opposite. It was found that the irreversibility increases with T_{HPG} in the HPG, LPG, condenser, expansion valve 3 (ExV3), SP, SHE1 and SHE2, particularly in the LPG, SP, ExV3 and the SHE2; there is a major increase in irreversibility at higher T_{HPG}. The irreversible losses in the three expansion valves (ExV1, ExV2 and ExV4), evaporator, absorber and the AC apparatus however were not changing with HPG temperature. Moreover, irreversible losses in ExV2 and ExV4 were zero and in the SP also, the irreversibility was negligible compared to the other components. The loss of exergy with the HPG leaving exhaust flue gas was also significantly high which increases with T_{HPG} due to loss of exergy at higher temperature. Among the double effect water−LiBr ARS components, the irreversibility was the maximum in the absorber at all HPG temperatures. Further, it was seen that the contribution of ARS components to total irreversibility changes with increase in T_{HPG}. At T_{HPG} =120°C, the next major contributor of irreversibility after the absorber was the evaporator. HPG, ARS condenser, SHE2, SHE1, LPG, ExV3, ExV1 and AC apparatus were the other components in sequential order in terms of its contribution to total irreversibility. However when T_{HPG} increases, at higher T_{HPG} i.e. at 150°C, the irreversibility distribution among the various ARS components changes. LPG irreversibility becomes significantly high and it becomes the second major contributor after the absorber followed by the evaporator, SHE2, HPG, ARS condenser, SHE1, ExV3, ExV1 and the AC apparatus. Gomri and Hakimi [13] in their study found that the absorber, HPG, SHE II, evaporator, SHE I, condenser and LPG were the components in sequential order in terms of their maximum contribution to total exergy. In this study, evaporator irreversibility was the next largest at T_{HPG} =120°C because of comparatively higher temperature difference between evaporating water at 10°C and incoming water at 25°C compared to that of Ref. [13]. Same was the reason of comparatively higher exergy loss in the condenser. Irreversibility in the LPG increases with T_{HPG} mainly due to increase in exergy at state points 10 and 11. Exergy at state points 12 and 14 also increases which however is not very significant compared to the

exergy increase at 10 and 11. Exergy at state point 15 does not change as T_{LPG} is fixed. The total irreversibility of the CS increases with T_{HPG} due to increase in irreversibility of HPG leaving flue gas, HPG, LPG, ARS condenser, expansion valve 3 (ExV3), SP, SHE1 and SHE2 of the bottoming ARS. Variation of total irreversibility with HPG temperature is shown in Fig. 6.3.

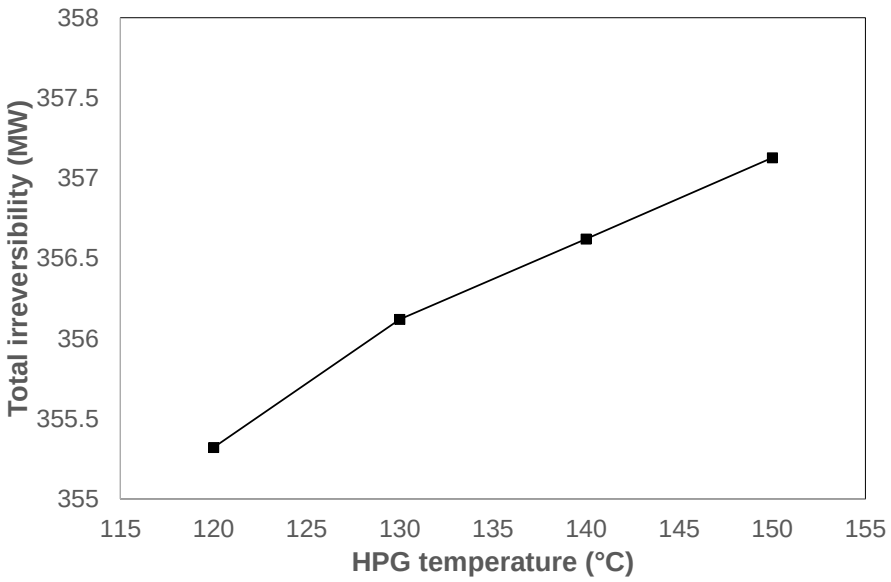

Fig. 6.3: Variation of total irreversibility of the combined power and cooling system with HPG temperature

In this study, it was also attempted to provide a performance comparison between the double effect water−LiBr ARS integrated CS and a CS integrated with flue gas operated single effect water−LiBr ARS. For comparing the two systems, it was considered that the flue gas leaves the PC boiler at 130°C in both the systems. T_{HPG} of the double effect ARS was considered 120°C while the generator temperature of the single effect ARS was taken 80°C. Performance comparison between the two systems is shown in Table 6.7. It was seen that the PC performance is not affected much due to replacement of the double effect ARS with the single effect ARS. Only the CT side pumping power increases, hence the net power output, energy and exergy efficiency of the topping PC decreases slightly. The EUF and exergetic efficiency of the CS also reduces slightly due to reduction in net power.

Table 6.7: Comparison of the double effect ARS (T_{HPG} =120°C, $T_{fg,HPGi}$ =130 °C, $T_{fg,HPGo}$ =123.61°C) integrated CS with and single effect ARS (T_G =80°C, $T_{fg,Gi}$ =130°C, $T_{fg,Go}$ =118.85°C) integrated CS

Performance parameters	Single effect	Double effect
Topping PC		
Net power (MW)	185.351	185.435
BFP pumping power (kW)	4233.471	4233.471
CT side pumping power (kW)	5674.147	5589.673
Steam generation rate (kg/s)	183.056	183.056
PC condenser loss (MW)	273.867	273.867
Energy efficiency of PC (%)	37.358	37.375
Exergy efficiency of PC (%)	35.225	35.241
CS		
EUF of the CS (%)	37.710	37.727
Exergetic efficiency of CS (%)	35.198	35.229
Bottoming ARS		
ARS COP	0.809	1.411
SP power (W)	0.0148	0.1405
$\dot{Q}_{HPG}$ (kW)	–	1240.167
$\dot{Q}_{LPG}$ (kW)	2163.895	1923.200
$\dot{Q}_C$ (kW)	1846.484	930.988
$\dot{Q}_A$ (kW)	2076.119	2076.119
Exergy efficiency	8.420	14.426

Obviously the COP of the double effect water−LiBr ARS is more and in this study also it was found that for the same evaporator CL of 500 ton (1750 kW), COP of the double effect ARS is 1.411 against a COP value of 0.809 of the single effect system. The SP pumping power was more in the double effect ARS due to high HPG pressure which was 43.062kPa compared to generator pressure (5.628 kPa) of the single effect ARS. The absorber pressure at 35°C was 1.228 kPa which was same in both the single and double effect ARS. The COP of double effect water−LiBr ARS was more due to the generator heat load which was less in the HPG of the double effect ARS (1240.167 kW)

compared to the generator heat load (2163.895 kW) of the single effect ARS. Magnitude of SP power is negligible compared to HPG heat load; hence COP of the double effect ARS becomes more in spite of its higher SP power. LPG heat load of the double effect ARS was also less compared to the generator heat load of the single effect ARS; the heat required for secondary vapor generation in the LPG was however provided by the HPG off primary vapour. The heat load in the condenser of the double effect system was also less which was about half of the condenser heat load of the single effect ARS. Therefore less amount of cooling water was required and hence the CT side pumping power was less in the CS with double effect ARS. The heat load in the absorber of the two systems was however the same. The exergy efficiency of the double effect water−LiBr ARS was found more (14.426%) than that of the single effect ARS (8.42%). This showed the advantage of the double effect ARS over the single effect system and not only from the first law but also from the second law point of view. This became clearer when the irreversibility in various system components of the CS integrated with double and single effect water−LiBr ARS were separately evaluated and compared. These are shown in Table 6.8. It was observed that the irreversibility in majority of the topping PC components does not change whether it is integrated with the double or the single effect ARS. Only in the MC2, CT and the CTPs, some changes occurred where irreversibility in the MC2 and CT was less while in the CTPs, the irreversibility was more in the double effect ARS than those of the single effect ARS. The main changes occurred in the irreversibility of the HPG and LPG of the double effect ARS. If the topping PC is integrated with the double effect ARS, the irreversibility in the HPG and LPG significantly reduces. The HPG and LPG irreversibility together was significantly less (30.297 kW and 4.861 kW respectively) compared to the generator irreversibility (250.889 kW) of the single effect system. Similarly the irreversibility in the condenser of the double effect system was also significantly less. The HPG temperature of the double effect ARS was 120°C whereas the generator temperature of the single effect ARS was 80°C. When the flue gas enters the generator of the single effect ARS at 130 °C, due to higher temperature difference (50°C), the irreversibility in the generator of the single effect ARS becomes significantly high.

Table 6.8: Comparison of components' irreversibility of the double effect ARS integrated CS with single effect ARS integrated CS

Component irreversibility (kW)	Notation	Single effect	Double effect
Topping PC			
Boiler	$\dot{I}_{boiler}$	222595.693	222595.693
Steam Turbine	$\dot{I}_{ST}$	20947.736	20947.736
PC condenser	$\dot{I}_{PCC}$	11242.480	11242.480
BFPs	$\dot{I}_{BFP}$	268.149	268.149
Open water heater	$\dot{I}_{OWH}$	4409.198	4409.198
Closed water heater	$\dot{I}_{CWH}$	3888.286	3888.286
Mixing chamber 1	$\dot{I}_{MC1}$	0	0
Mixing chamber 2	$\dot{I}_{MC2}$	270.222	244.712
Cooling tower	$\dot{I}_{CT}$	17749.173	17726.555
Cooling tower pumps	$\dot{I}_{CTP}$	21272.269	21577.971
Bottoming ARS			
HP Generator	$\dot{I}_{HPG}$	–	30.152
LP Generator	$\dot{I}_{LPG}$	250.440	4.861
VARS condenser	$\dot{I}_{C}$	48.684	24.392
Expansion valve 1	$\dot{I}_{ExV1}$	3.390	3.390
Expansion valve 2	$\dot{I}_{ExV2}$	0.000	0
Expansion valve 3	$\dot{I}_{ExV3}$	–	4.325
Expansion valve 4	$\dot{I}_{ExV4}$	–	0
Evaporator	$\dot{I}_{E}$	47.125	47.125
Absorber	$\dot{I}_{A}$	101.965	101.992
Solution pump	$\dot{I}_{SP}$	0.014	0.1305
Solution heat exchanger 1	$\dot{I}_{SHE1}$	11.346	11.354
Solution heat exchanger 2	$\dot{I}_{SHE2}$	–	17.594
AC apparatus	$\dot{I}_{AC}$	1.724	1.724
Exhaust gas	$\dot{I}_{fg}$	50478.700	52173.419
Total irreversibility		353586.594	355321.238

Contrary to this, the temperature difference between the flue gas and HPG temperature of the double effect system is less (10°C), hence irreversibility in the HPG reduces. Irreversibility in the generator of single effect ARS can be reduced by lowering the inlet flue gas temperature. However, if $T_{fg,Gi}$ is lowered $T_{fg,Go}$ will also decrease

simultaneously and this may lead to sulphur corrosion hazard at the cold end of the boiler at lower temperature. In order to avoid cold end corrosion, the boiler heat transfer surface leaving gas temperature in thermal power plants is kept in the range from 115°C to 160°C. Irreversibility in the condenser of the double effect was less due to the following reasons. Refrigerant mass flow rate (0.737 kg/s) and exergy of condenser leaving liquid refrigerant were the same in both the single and double effect ARS. Specific exergy of the vapour stream at condenser inlet was also the same in the two systems, however the mass flow rate of vapor entering the condenser was different which in the single effect system was same as that of refrigerant flow rate while in the double effect system it was comparatively less. Therefore, the vapour exergy at condenser inlet became less in the double effect system. There was also significant difference in the condenser cooling water mass flow rate of the two systems; the flow rate of cooling water in the single effect system was almost double of the flow rate of the double effect system due to its higher $\dot{Q}_C$ value. The net rate of exergy efflux with condenser cooling water which is a negative quantity was thus more in the single effect ARS. Although the negative value of cooling water exergy efflux was comparatively less and the exergy with respect to the state point $13'$ was an extra term in the double effect system, but the lower value of vapour exergy at condenser entry was mainly responsible for lower condenser irreversibility of the double effect system.

Since the generator heat load was more in the single effect ARS and also the flue gas entered the HPG of the double effect and generator of the single effect ARS at the same temperature (130°C), therefore the flue gas temperature at generator outlet of the single effect ARS became less (118.85°C) than the HPG outlet flue gas temperature of the double effect system (123.61°C). The flue gas in the HPG of the double effect ARS cannot be cooled below 120°C as there will be reverse heat transfer and a minimum temperature difference of 3°C is often desirable, hence a flue gas temperature of 123.61°C at HPG outlet of the double effect ARS is acceptable from this point of view. Since the flue gas leaves the HPG of the double effect ARS at higher temperature, therefore the exergy loss with the HPG leaving flue gas was more in the double effect ARS. Irreversibility in the SP of the double effect ARS was also more than that of the single effect system. Loss of exergy in the SHE2 and ExV3 were additional in the double effect ARS. Consequently the total irreversibility of the double effect ARS integrated combined power and cooling system was more although in some of the components

(HPG and ARS condenser) the irreversible losses were significantly less than those of the single effect system.

6.7 Summary

A combined vapor power cycle and double effect H_2O–LiBr ARS is proposed. The double effect ARS is driven by flue gas of the vapor power cycle. Energy and exergy balance equations are applied to various system components to determine energetic and exergetic performance of the PC, ARS and the combined power and cooling system as a whole. A parametric study is performed to investigate the effect of variation of HPG and flue gas temperature on performance of the combined system. Based on the findings, the following conclusions are made.

1. A double effect H_2O–LiBr ARS may be integrated in a ST based PC to achieve power and cooling simultaneously in a cogeneration mode by utilizing the exhaust heat of the boiler leaving flue gas to drive the HPG of the double effect ARS. With the chosen operating conditions, the PC generates a net power of approximately 185 MW and simultaneously it also produces 500 ton (1750 kW) of cooling at T_{HPG} =120°C.

2. Parametric study showed that the net power and efficiency of the topping PC reduces with increase in T_{HPG} due to reduction in steam generation rate in the boiler. COP and exergy efficiency of the double effect ARS also decreases with T_{HPG}. The EUF and exergy efficiency of the combined power and cooling system also shows a declining trend with increasing T_{HPG}. However it is possible to have more tonnage of cooling from the bottoming ARS at higher T_{HPG}.

3. The irreversible losses in the PC components decrease with T_{HPG} while in the ARS components, particularly in the LPG, SP, ExV3 and the SHE2; irreversibility shows a major increase at higher T_{HPG}. The exergy loss with the HPG leaving flue gas also increases with T_{HPG}. The total irreversibility of the CS increases with T_{HPG} due to increase in HPG leaving flue gas irreversibility and irreversibility insome of the double effect ARS components.

4. Among the ARS components, maximum irreversibility occurs in the absorber. Further it was observed that the contribution of ARS components to total irreversibility changes with T_{HPG}. Evaporator, HPG, condenser, SHE2, SHE1 and the LPG are the next major contributors of irreversibility at T_{HPG} =120°C. However when T_{HPG} increases, at T_{HPG} =150°C, LPG becomes the second major contributor after the absorber followed by the evaporator, SHE2, HPG, ARS condenser and SHE1.

5. The double effect ARS would be more appropriate for integration with the PC. Comparison between the double and single effect ARS integrated CS showed that the net power and efficiencies of the topping PC decreases when the PC is integrated with the single effect ARS. Higher COP and exergy efficiency of the double effect ARS are obtained with lower irreversibility in the HPG and condenser. Further it was observed that the sum of components' irreversibility (excluding flue gas exergy at HPG exit) was almost the same in both the systems, although the number of components in the double effect ARS was more.

List of References

[1] Vliet, G. C., Lawson, M. B., and Lithgow, R. A. Water lithium bromide double–effect absorption cooling cycle analysis. *ASHRAE Transaction*, 88:811–822, 1982.

[2] Farshi,L.G., Mahmoudi,S. M. S., and Rosen,M.A. Analysis of crystallization risk in double effect absorption refrigeration systems. *Applied Thermal Engineering*, 31(10):1712–1717, 2011.

[3] Farshi,L.G., Mahmoudi, S. M. S., Rosen, M. A., and Yari, M. A comparative study of the performance characteristics of double-effect absorption refrigeration systems. *International Journal of Energy Research*, 36(2):182–192, 2012.

[4] Arun, M. B., Maiya, M. P., and Murthy, S .S. Equilibrium low pressure generator temperatures for double–effect series flow absorption refrigeration systems. *Applied Thermal Engineering*, 20:227–242, 2000.

[5] Arun,M.B., Maiya,M.P., and Murthy,S.S. Performance comparison of double–effect parallel–flow and series flow water–lithium bromide absorption systems. *Applied Thermal Engineering*, 21(12): 1273–1279, 2001.

[6] Kaushik, S. C., and Chandra, S. Computer modelling and parametric study of a double–effect generation absorption refrigeration cycle. *Energy Conversion and Management*, 25:9–14, 1985.

[7] Liu, Y. L. and Wang, R. Z. Performance prediction of a solar/gas driving double effect LiBr–H_2O absorption system.*Renewable Energy*, 29:1677–1695, 2004.

[8] Torrella, E., Sánchez, D., Cabello, R., Larumbe, J. A., and Llopis, R. On–site real–time evaluation of an air–conditioning direct–fired double–effect absorption chiller, *Applied Energy*, 86: 968–975, 2009.

[9] Xu, G. P., Dai, Y. Q., Tou, K. W., and Tso, C. P. Theoretical analysis and optimization of a double–effect series–flow–type absorption chiller. *Applied Thermal* Engineering, 16:975–987, 1997.

[10] Xu, G. P. and Dai, Y. Q.Theoretical analysis and optimization of a double–effect parallel–flow–type absorption chiller. *AppliedThermal Engineering*, 17(2): 157–1 70, 1997.

[11] Yin, H., Qu, M., and Archer, D. H. Model based experimental performance analysis of a microscale LiBr–H_2Osteam–drivendouble–effect absorption chiller. *Applied Thermal Engineering*, 30:1741–1750, 2010.

[12] Figueredo, G. R., Bourouis, M., and Coronas, A. Thermodynamic modelling of a two–stage absorption chiller driven at two–temperature levels. *Applied Thermal Engineering*, 28(2–3): 211–217, 2008.

[13] Gomri, R. and Hakimi, R. Second law analyses of double effect vapour absorption cooler system. *Energy Conversion and Management*,49(11):3343–3348, 2008.

[14] Gomri, R. Second law comparison of single effect and double effect vapour absorption refrigeration systems. *Energy Conversion and Management*, 50:1279–1287, 2009.

[15] Gomri, R. Investigation of the potential of application of single effect and multiple effect absorption cooling systems. *Energy Conversion and Management*, 51:1629–1636, 2010.

[16] Kaushik, S. C. and Arora, A. Energy and exergy analysis of single effect and series flow double effect water–lithium bromide absorption refrigeration Systems. *International Journal of Refrigeration*,32:1247–1258, 2009.

[17] Khaliq, A., and Kumar, R.Exergy analysis of double effect vapor absorption refrigeration system. *International Journal of Energy Research*, 32: 161–174, 2008.

[18] Ravikumar, T. S., Suganthi, L., and Anand, A. S.Exergy analysis of solar assisted double effect absorption refrigeration system. *Renewable Energy*, 14: 55–59, 1998.

[19] Adewusi, S. A. and Zubair, S. M. Second law based thermodynamic analysis of ammonia–water absorption systems. *Energy Conversion and Management*,45(15–16): 2355–2369, 2004.

[20] Farshi, L.G., Mahmoudi, S. M. S., Rosen, M. A., Yari,M., and Amidpour, M. Exergoeconomic analysis of double effect absorption refrigeration systems. *Energy Conversion and Management*,65:13–25, 2013.

[21] Gebreslassie,B.H., Medrano,M., and Boer,D. Exergy analysis of multi–effect water–LiBr absorption systems: from half to triple effect. *Renewable Energy*, 35(8):1773–1782, 2010.

[22] Gomri, R. Thermodynamic evaluation of triple effect absorption chiller. In *Thermal Issues in Emerging Technologies* (ThETA 2), Cairo, Egypt, 17–20thDec 2008.

[23] Jiang, L., Gu, Z., Feng, X., and Li, Y. Thermo–economical analysis between new absorption–ejector hybrid refrigeration system and small double–effect absorption system. *Applied Thermal Engineering*, 22: 1027–1036, 2002.

[24] Li, Z. and Liu, J. Appropriate heat load ratio of generator for different types of aircooled lithium bromide–water double effect absorption chiller. *Energy Conversion and Management*, 99:264–273, 2015.

[25] Manohar, H. J., Saravanan, R., and Renganarayanan,S.Modelling of steam fired double effect vapour absorption chiller using neural network. *Energy Conversion and* Management, 47: 2202–2210, 2006.

[26] Shin, Y., Seo, J. A., Cho, H. W., Nam, S. C., and Jeong, J. H. Simulation of dynamics and control of a double–effect LiBr–H_2O absorption chiller. *Applied Thermal Engineering*, 29:2718–2725, 2009.

[27] Abu–Ein,S.Q.,Fayyad, S. M., Momani, W., and Al–Bousoul, M. Performance analysis of solar powered absorption refrigeration system. *Heat and Mass Transfer*,46:137–145, 2009.

[28] Assilzadeh,F.,Kalogirou, S. A., Ali, Y., and Sopian, K. Simulation and optimization of a LiBr solar absorption cooling system with evacuated tube collectors. *Renewable Energy*,30(8): 1143–1159, 2005.

[29] Florides,G.A.,Kalogirou, S. A., Tassou, S. A., and Wrobel, L. C. Modelling and simulation of an absorption solar cooling system for Cyprus. *Solar Energy*, 72(1): 43–51, 2002.

[30] Mittal,V., Kasana, K. S., and Thakur, N. S. Performance evaluation of solar absorption cooling system of Bahal (Haryana). *Journal of Indian Institute of Science*, 85: 295–305, 2005.

[31] Li, Z., Ye, X.,and Liu, J. Performance analysis of solar air cooled double effect LiBr/H_2Oabsorption cooling system in subtropical city. *Energy Conversion and Management*, 85:302–312, 2014.

[32] Havelsky V. Energetic efficiency of cogeneration systems for combined heat, cold and power production. *International Journal of Refrigeration*, 22(6):479–485, 1999.

[33] Huangfu, Y., Wu, J. Y., Wang, R. Z., Kong, X. Q.,and Wei, B. H. Evaluation and analysis of novel micro–scale combined cooling, heating and power (MCCHP) system. *Energy Conversion and Management*, 48:1703–1709, 2007.

[34] Manzela, A. A., Hanriot, S. M., Cabezas–Gomez, L., and Sodre, J. R. Using engine exhaust gas as energy source for an absorption refrigeration system. *Applied Energy*, 87(4):1141–1148, 2010.

[35] Mostafavi, M. and Agnew,B. Thermodynamic analysis of combined diesel engine and absorption refrigeration unit—naturally aspirated diesel engine. *Applied Thermal Engineering*, 17(5):471–478, 1997.

[36] Ouadha, A. and El–Gotni, Y. Integration of an ammonia–water absorption refrigeration system with a marine Diesel engine: A thermodynamic study. *Procedia Computer Science*, 19:754–761, 2013.

[37] Rêgo,A.T., Hanriot,S.M., Oliveira,A.F., Brito,P., and Rêgo,T.F.U. Automotive exhaust gas flow control for an ammonia–water absorption refrigeration system. *Applied Thermal Engineering*, 64(1–2):101–107, 2014.

[38] Talbi, M. and Agnew,B. Energy recovery from diesel engine exhaust gases for performance enhancement and air conditioning. *Applied Thermal Engineering*, 22(6):693–702, 2002.

[39] Ameri, M. and Hejazi,S.H. The study of capacity enhancement of the Chabahar gas turbine installation using an absorption chiller. *Applied Thermal Engineering*, 24(1):59–68, 2004.

[40] Bruno,J.C., Valero,A., and Coronas,A. Performance analysis of combined microgas turbines and gas fired water/LiBr absorption chillers with post–combustion. *Applied Thermal Engineering*, 25(1): 87–99, 2005.

[41] Bruno, J. C., Ortega–López, V., and Coronas, A. Integration of absorption cooling systems into micro gas turbine trigeneration systems using biogas: case study of a sewage treatment plant. *Applied Energy*, 86:837–849, 2009.

[42] Colonna, P. and Gabrielli,S. Industrial trigeneration using ammonia–water absorption refrigeration systems (AAR).*Applied Thermal Engineering*, 23(4):381–396, 2003.

[43] Huicochea, A., Rivera,W., Gutiérrez–Urueta, G., Bruno,J.C., and Coronas,A. Thermodynamic analysis of a trigeneration system consisting of a micro gas turbine and a double effect absorption chiller. *Applied Thermal Engineering*, 31(16):3347–3353, 2011.

[44] Hwang, Y. Potential energy benefits of integrated refrigeration system with microturbine and absorption chiller. *International Journal of Refrigeration*, 27:816–829, 2004.

[45] Khaliq,A. Exergy analysis of gas turbine trigeneration system for combined production of power heat and refrigeration. *International Journal of Refrigeration*, 32(3):534–545, 2009.

[46] Martins, L. N., Fábrega, F. M., d'Angelo, J. V. H. Thermodynamic performance investigation of a trigeneration cycle considering the influence of operational variables. *Procedia Engineering*, 42:1879–1888, 2012.

[47] Moné,C.D., Chau,D.S., and Phelan,P.E. Economic feasibility of combined heat and power and absorption refrigeration with commercially available gas turbines. *Energy Conversion and Management*, 42(13): 1559–1573, 2001.

[48] Moran,M.J. ,and Shapiro, H.N. *Fundamental of engineering thermodynamics*, Singapore: John Wiley & Sons, 4th edition,2005.

[49] Patek, J.,and Klomfar, J. A computationally effective formulation of thermodynamic properties of LiBr–H_2O solutions from 273 to 500 K over full composition range. *International Journal of Refrigeration*, 29:566–578, 2006.

[50] Lansing, F.L. Computer modelling of a single stage lithium bromide/water absorption refrigeration unit, JPL Deep Space Network progress Report 42–32, DSN Engineering section.247–257, 1976.